Development and validation of a real-time model for the simulation of the heat release rate, in-cylinder pressure and pollutant emissions in diesel engines

15JENG-0089

Development and Validation of a Real-Time Model for the Simulation of the Heat Release Rate, In-Cylinder Pressure and Pollutant Emissions in Diesel Engines

Roberto Finesso, Ezio Spessa, and Yixin Yang
Politecnico di Torino

Abstract

A real-time mean-value engine model for the simulation of the HRR (heat release rate), in-cylinder pressure, brake torque and pollutant emissions, including NOx and soot, has been developed, calibrated and assessed at both steady-state and transient conditions for a Euro 6 1.6L GM diesel engine.

The chemical energy release has been simulated using an improved version of a previously developed model that is based on the accumulated fuel mass approach. The in-cylinder pressure has been evaluated on the basis of the inversion of a single-zone model, using the net energy release as input. The latter quantity was derived starting from the simulated chemical energy release, and evaluating the heat transfer of the charge with the walls. NOx and soot emissions were simulated on the basis of semi-empirical correlations that take into account the in-cylinder thermodynamic properties, the chemical energy release and the main engine parameters.

The model is also referred to as “steady-state” as the main thermodynamic properties in the intake and exhaust manifolds, as well as the inducted mass flow rate, have been evaluated by means of correlations that were calibrated under steady-state conditions. This has allowed a very low computational time to be obtained, so that the approach is suitable for implementation in an ECU for real-time applications.

The model has been calibrated over several experimental tests carried out at a dynamic test bench at GMPT-E (General Motors powertrain-Europe). The tests include a complete engine map as well as several full-factorial variation lists of the main engine parameters, which have been conducted for seven representative operating conditions of the NEDC (New European Driving Cycle).

The validation has been carried out under transient conditions over NEDC and WLTP missions, which were simulated at the dynamic test bench for a C-class vehicle.

Introduction

The increasing computational capabilities of modern ECUs (Engine Control Units) in diesel engines are offering the opportunity of implementing more and more complex model-based algorithms in order to control the combustion and pollutant formation processes in real time.

The development of real-time models that focus on these aspects is therefore of great interest for car manufacturers. However, these fast and reliable simulation tools should also be able to realize an offline optimization of the main engine parameters, in order to reduce the experimental effort and the related costs.

In general, the simulation of the fluid-dynamics in the pipes, manifolds and in the combustion chamber, as well as of the combustion and emission formation processes, can be carried out with different degrees of detail, using multidimensional, one-dimensional or zero-dimensional approaches.

3D-CFD (Computer Fluid-Dynamics) calculation methods a priori have the potential of reproducing the physical and chemical processes that take place in the engine pipes, as well as in the chamber during the injection-combustion process, but they require a considerable computational time and suffer from the drawback of still being conditioned by a lack of precise knowledge on the physics of some processes. These methods therefore usually focus on the simulation of specific engine sub-systems. For example, 3D-CFD simulations have been applied to identify the optimal geometry of the intake manifold in [1], or to optimize the engine water cooling jacket in [2], where the CFD code has been used in conjunction with an FEM (Finite Element Method) tool for the structural analysis. However, the main application fields of 3D-CFD simulations in diesel engines are mainly focused on the in-cylinder processes, including spray formation [3], mixture preparation [4], as well as combustion and pollutant formation [5-9].

The complete simulation of the pipes and intake/exhaust manifolds of the engine system is usually carried out with 1D-CFD models coupled with a zero-dimensional modeling of the cylinders, injectors, valves, compressors and turbines. The 1D approach is based on the application of the conservation equations for the unsteady compressible flows in the pipes, and it allows the wave propagation phenomena, as well as the inertial effects, to be captured in steady-state and transient conditions. Several examples of studies based on this approach can be found in the literature [10-13]. However, this approach cannot be applied for real-time applications, as it requires a computational time of the order of several minutes to simulate a single operating condition on a modern PC. The modeling of the intake and exhaust manifolds could be simplified using lumped parameter approaches, such as those presented in [14], in which the manifolds are treated as single control volumes to which mass and energy conservation laws are applied. This approach requires a much lower computational effort than the 1D approach. However, differential equations for the control volumes still have to be solved.

Given this background, a mean-value zero-dimensional engine model for real-time applications has been developed in this study.

The model includes the simulation of the HRR (heat release rate), of the in-cylinder pressure and of the related combustion parameters, including peak firing pressure (PFP), indicated mean effective pressure (IMEP), friction mean effective pressure (FMEP), brake mean effective pressure (BMEP), as well as of the NOx and soot emissions.

Several approaches have been proposed in the literature to simulate the HRR. For example, the shape of the HRR can be predicted by means of mathematical functions, including those of Wiebe [15-17]. Although widely used, this is a purely mathematical approach that lacks physical consistency. Another proposed methodology to simulate HRR in diesel engines is based on the apparent combustion time [18-19]. This is a phenomenological approach that is capable of taking into account the effects of the influence of the in-cylinder air density, oxygen concentration, nozzle diameter and injection rate. Finally, one of the most widely adopted methods to simulate heat release is the accumulated fuel mass approach [20-24]. This method is based on the assumption that the rate of released chemical energy is proportional to the energy associated with the fuel quantity made available for combustion at the considered instant. This energy can be computed at time t as the difference between the chemical energy associated with the injected fuel quantity and the cumulative heat release. This method has the great advantage of being able to directly relate the injection rate to the combustion rate, and is therefore physically consistent.

A predictive real-time combustion model, based on the accumulated fuel mass approach, has already been presented by the authors in [24]. In that case, the HRR model was coupled with a single zone approach to simulate the in-cylinder pressure, but it required the measurement of the intake/exhaust manifold thermodynamic quantities, as well as of the inducted mass flow rate, and did not include a friction model to predict BMEP.

The engine model proposed in this study starts from the approach proposed in [24] and includes the following novelties:

- An enhanced version of the HRR model has been used. This model has recently been developed and proposed by the authors in [25]; in the present study, the improvements in the prediction of the in-cylinder pressure and pollutant emissions have been evaluated using the enhanced heat release model instead of the previous model presented in [24].

- Correlations calibrated at steady-state engine operating conditions have been introduced in order to evaluate the intake and exhaust manifold thermodynamic conditions, as well as the inducted charge mass.

- A correlation has been identified to evaluate the EGR (Exhaust Gas Recirculation), starting from the EGR valve and throttle valve opening signals, as well as from the thermodynamic quantities in the intake/exhaust manifolds; this has allowed the intake oxygen concentration to be evaluated.

- A friction model, which is based on the Chenn-Flynn approach, has been implemented in order to predict FMEP; this has allowed BMEP to be evaluated on the basis of the IMEP.

- Semi-empirical models, previously developed in [26,27], have been assessed and tuned in order to predict NOx and soot emissions, which are the most critical pollutant species in diesel engines.

The model was calibrated over several experimental tests carried out at a dynamic test bench at GMPT-E (General Motors powertrain-Europe). The tests include a complete engine map as well as several full-factorial variation lists of the main engine parameters, which were conducted for seven representative operating conditions of the NEDC (New European Driving Cycle).

After the tuning, the model performance was evaluated under steady-state and transient conditions. In particular, the main combustion parameters, i.e., MFB50 (crank angle at which 50% of the fuel mass has burnt), PFP, IMEP, as well as the NOx emissions were compared with the experimental trends over NEDC and WLTP missions. The results obtained with the developed engine model were compared with those obtained with the same combustion and NOx formation models, but using the measured intake/exhaust variables during the transients instead of the values obtained with the steady-state correlations. The aim of this comparison was to verify whether the assumption of using steady-state correlations to estimate the intake/exhaust variables could be accepted when simulating moderately transient conditions, such as the NEDC/WLTP cycles.

Finally, a sensitivity analysis was carried out on the calculation step and on the number of experimental tests required for model calibration.

The developed model can be useful for several applications, such as offline calibration of engine parameters, engine simulation in Hardware-in-the-Loop (HiL) or Model-in-the-Loop (MiL) systems, as well as development of model-based feed-forward control algorithms.

Engine setup and experimental activity

The experimental tests for the calibration and validation of the models were conducted on a 1.6L Euro 6 diesel engine. The main engine technical specifications are summarized in Tab. 1.

Table 1. Main engine specifications.

Engine type	Euro 6 diesel engine
Displacement	1598 cm^3
Bore x stroke	79.7 mm x 80.1 mm
Rod length	135 mm
Compression ratio	16.0
Valves per cylinder	4
Turbocharger	VGT type
Fuel injection system	Common Rail
Specific power and torque	71 kW/l – 205 Nm/l

The engine is equipped with a short-route cooled EGR system, in which the EGR valve is located upstream from the cooler. A throttle valve is installed upstream from the intake manifold and EGR junction, in order to allow high EGR rates to be obtained when the pressure drop between the exhaust and intake manifolds is not sufficient. Moreover, the EGR circuit is equipped with an EGR

cooler bypass, in order to prevent EGR gases from flowing across the cooler under certain driving conditions, e.g., during cold start phases.

The test engine was instrumented with piezoresistive pressure transducers and thermocouples to measure the pressure and temperature at different locations, such as upstream and downstream from the compressor, turbine and intercooler, and in the intake manifold. Thermocouples were also used to measure the temperatures in each exhaust runner. Piezoelectric transducers were installed to measure the pressure time-histories in the combustion chamber of the cylinders.

The experimental tests were carried out on a dynamic test bench at GMPT-E, in the frame of a research project between the Politecnico di Torino and GMPT-E, pertaining to the assessment of control-oriented heat release predictive models [25]. To this aim, several tests were conducted, including:

- Full-Factorial variation tests of p_{int} (intake manifold pressure), SOI_{main} (start of injection of the main pulse), O_2 (intake oxygen concentration) and p_f (injection pressure) at several representative key-points of the NEDC cycle.

- A full engine map with baseline operating parameters.

Table 2 summarizes the experimental test matrix used for the calibration of the models, and reports the minimum and maximum values of the main engine parameters for the different operating points.

Table 2. Experimental test matrix.

Operating point	Tests		p_f	p_{int}	O_2	λ	X_r	q_{pil2}	q_{pil1}	$q_{f,inj}$	SOI pil2	SOI pil1	SOI main
			bar		%	-		mm^3	mm^3	mm^3	CAD	CAD	CAD
1500x2	100	max	500	1.26	20.6	4.78	50.1	1.3	1.6	9.18	332.7	342.6	353.2
		min	250	0.95	14.7	1.65	0.98	1.3	1.5	7.74	339.4	348.5	358.2
1500x5	100	max	680	1.45	20.7	2.81	36.5	1.3	1.6	17.8	331.5	340.7	352.9
		min	380	0.95	14.4	1.14	0.53	1.3	1.6	15.4	339.5	348.5	358.2
1500x8	100	max	800	1.68	20.8	2.18	17.9	1.3	1.6	28.1	331.4	340.0	355.5
		min	400	1.10	18.1	1.11	0.32	1.3	1.6	23.4	337.9	346.4	360.0
2000x2	100	max	580	1.58	20.73	5.13	48.2	1.3	1.5	10.1	327.4	339.8	354.7
		min	250	0.85	15.3	1.63	0.71	1.3	1.5	7.90	332.8	343.8	356.6
2000x5	100	max	680	1.87	20.7	3.48	30.5	1.3	1.5	17.1	326.8	338.3	354.8
		min	380	0.97	16.4	1.3	0.47	1.3	1.5	15.0	329.8	340.7	355.4
2000x8	100	max	1100	2.09	20.8	2.64	21.0	1.3	1.5	26.6	325.1	335.9	356.1
		min	700	1.34	17.2	1.17	0.45	1.3	1.5	23.4	326.8	337.2	356.4
2000x12	100	max	1040	2.46	20.8	2.18	0.47	1.3	1.8	36.1	326.2	338.7	351.5
		min	640	1.84	20.8	1.75	0.33	1.3	1.8	33.5	327.3	339.3	351.5
Engine map	285	max	1936	2.73	20.8	5.77	50.6	1.3	3.1	74.0	311.5	306.3	337.5
		min	305	1.01	16.8	1.08	0.14	0	1.3	5.47	360.0	353.4	360.2

The key-points are identified by the speed and BMEP (rpm x bar) values. X_r is the EGR rate, defined as the ratio between the inducted EGR mass flow rate and the total inducted mass flow rate; λ is the relative air-to-fuel ratio, q_{pil2} and q_{pil1} indicate the injected fuel quantity of the pilot2 and pilot1 injections, respectively, while $q_{f,inj}$ denotes the total injected fuel quantity. All injected quantities are expressed in mm^3/cyc.

Figure 1 reports the engine map tests, in terms of normalized BMEP and engine speed.

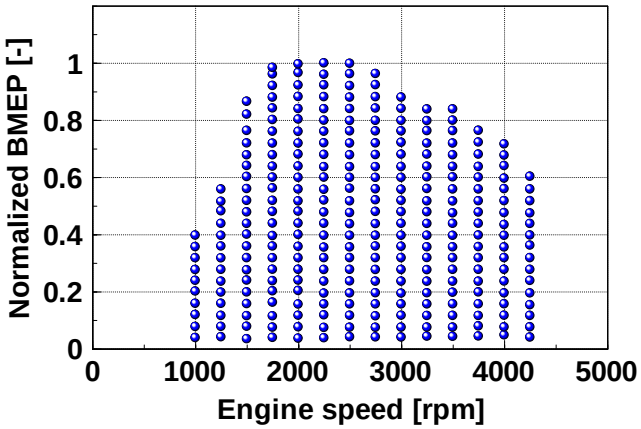

Figure 1. Engine map tests used for the calibration of the models.

REAL-TIME ENGINE MODEL

The real-time model proposed in this study includes the simulation of:

1. Chemical energy release: the approach is based on an enhanced version (see [25]) of the model previously presented by the authors, which was based on the accumulated fuel mass approach [24]. The input data of the model are the injection parameters, as well as the main thermodynamic conditions in the intake manifold and the engine operating parameters.

2. In-cylinder pressure: the approach is based on the inversion of a single-zone heat release model which requires the net energy release as input; the latter is derived starting from the predicted chemical energy release and estimating the heat transfer between the charge and the walls. Polytropic evolutions are assumed during the compression and expansion phases. The simulation of the in-cylinder pressure allows several parameters, such as PFP and IMEP, to be evaluated.

3. Friction losses: the Chenn-Flynn approach has been used to predict FMEP on the basis of the engine speed and PFP; the simulation of FMEP allows BMEP to be evaluated starting from IMEP.

4. EGR rate: the EGR rate has been modeled by means of an empirical correlation that estimates the in-cylinder trapped EGR volume on the basis of the opening position of the EGR valve, of the thermodynamic conditions upstream and downstream from the valve, of the cooler by-pass activation flag and of the throttle valve position. The simulation of the EGR rate is required to evaluate the intake oxygen concentration, which is then used in several correlations.

5. NOx and soot emission levels: the semi-empirical correlations previously developed by the authors for a 2.0L Euro 5 diesel engine and reported in [26, 27] have been tuned and validated for the 1.6L Euro 6 engine considered in the present study.

6. Intake/exhaust manifold thermodynamic conditions and inducted mass flow rate: a steady-state approach has been applied in the present study, and neither the turbocharger nor the intake and exhaust manifolds have been simulated. The pressure in the intake manifold (p_{int}) has been set equal to the set-point value that was derived from the baseline engine map, as a function of the engine load and speed; the intake manifold temperature has been evaluated by means of an

enthalpy balance equation at the EGR mixing node; the exhaust manifold temperature has been evaluated by means of a correlation that takes into account the in-cylinder temperature at exhaust valve opening, as well as the engine load and speed; the exhaust manifold pressure has been evaluated by means of a look-up table that takes into account the pressure in the intake manifold, the engine load and speed. The inducted charge mass has been evaluated on the basis of the volumetric efficiency, which was evaluated on the basis of a look-up table.

The main advantage of this approach consists in the high computational time saving, which makes it suitable for implementation in an ECU for real-time applications.

The main drawbacks of such an approach are related to the fact that the lags due to the delayed response of the turbocharger, as well as the effects related to the filling and emptying processes of the manifolds and the high pressure EGR delays are not taken into account. The proposed method is therefore not expected to provide an accurate simulation of fast transient conditions. However, one of the objectives of the present study is to verify whether this approach is suitable for simulating moderately transient conditions, such as the NEDC/WLTP cycles.

A summary of each sub-model is reported hereafter.

In general, it should be pointed out that the HRR and in-cylinder pressure models were assessed on the basis of the measured in-chamber pressure of one of the four cylinders, which was considered as the representative one. It was in fact verified that the cylinder-to-cylinder dispersion of the main combustion parameters is low.

Estimation of the chemical energy release Q_{ch}

The chemical energy release has been simulated on the basis of an enhanced version [25] of the baseline model presented by the authors in [24], which was based on the accumulated fuel mass approach.

The accumulated fuel mass approach assumes that, at any time instant, the rate of chemical energy released by the fuel is proportional to the energy associated with the in-cylinder accumulated fuel mass. Such an energy can be calculated at time instant t as the difference between the chemical energy of the injected fuel mass and the released chemical energy.

It was verified in [25] that this approach leads to accurate results for the pilot injections, for which the chemical energy release rate has therefore been evaluated as follows:

$$\frac{dQ_{ch,pil,j}}{dt}(t) = K_{pil,j}\left[Q_{fuel,pil,j}(t-\tau_{pil,j}) - Q_{ch,pil,j}(t)\right] \quad (1)$$

where $K_{pil,j}$ and $\tau_{pil,j}$ are model calibration quantities related to the combustion rate and to the ignition delay, respectively, and $Q_{fuel,pil,j}$ is the chemical energy associated with the injected fuel mass.

The chemical energy release of the main pulse has instead been simulated by means of a modified formulation that was proposed in [25], and which leads to a higher accuracy especially at medium-high load conditions:

$$\frac{dQ_{ch,main}}{dt}(t) = K_{1,main}\left[Q_{fuel,main}(t-\tau_{main}) - Q_{ch,main}(t)\right] + K_{2,main}\frac{dQ_{fuel,main}(t-\tau_{main})}{dt} \quad (2)$$

The formulation proposed in Eq. (2) needs an additional calibration parameter with respect to the baseline approach of Eq. (1) (i.e., $K_{2,main}$).

From a physical point of view, the term proportional to the injection rate takes into account the effect, on the heat release, of the turbulence induced by the fuel injection, which is not negligible in diesel sprays.

For each injection pulse j, the chemical energy Q_{fuel} associated to the injected fuel quantity is defined as follows:

$$Q_{fuel,j}(t) = \int_{t_{SOI,j}}^{t} \dot{m}_{f,inj}(t) H_L dt \qquad t \le t_{EOI,j} \quad (3)$$

$$Q_{fuel,j}(t) = \int_{t_{SOI,j}}^{t_{EOI,j}} \dot{m}_{f,inj}(t) H_L dt \qquad t > t_{EOI,j} \quad (4)$$

where t_{SOI} is the start of the injection time, t_{EOI} the end of the injection time, H_L the lower heating value of the fuel and $\dot{m}_{f,inj}$ the fuel mass injection rate.

The total chemical energy release is given by the sum of the contributions of all the injection pulses:

$$Q_{ch} = \sum_{j=1}^{n} Q_{ch,j} \quad (5)$$

It can be noted, from Eqs. (1-2), that the baseline approach described in [24] has been used for the pilot shots, as it had been verified that it provides satisfactory results [25].

Instead, an enhanced formulation, which includes an additional term proportional to the injection rate, has been developed for the main pulse. It had been verified in [25] that the addition of this term leads to an increase in the accuracy of the predicted heat release trend and of MFB50, especially at high-load operating conditions, where the combustion of the main pulse is of the premixed/mixing-controlled type.

The term proportional to the injection rate takes into account the effect of the injection-induced turbulence on the heat release, which is a non-negligible term in diesel sprays which influences the mixing controlled combustion phase that usually occurs during the oxidation of the main pulse.

The model was assessed for the steady-state conditions reported in Tab. 2. In particular, the optimal τ and K parameters were identified by comparing the predicted and experimentally-derived heat release profiles, and minimizing the sum of errors and the MFB50 prediction error by means of a genetic algorithm (see [25]). The adopted correlation variables for ignition delay were chosen in accordance

with the study proposed in [28]. In particular, at the beginning, all the engine variables were included in the correlations, and a sensitivity analysis was carried out in order to exclude the least influential ones, thus a stepwise regression was adopted. This approach was also adopted to identify the engine variables that had to be included in all the correlations reported hereafter.

The following correlations were identified in [25] as a function of the in-chamber thermodynamic quantities at SOI/SOC (start of injection/start of combustion) and other engine variables:

$$K_{pil}\left[\frac{1}{s}\right] = 1.109\, exp\left(\frac{-10254}{T_{SOC,pil}}\right) O_2^{3.80} n^{0.724} q_{pil,tot}^{-0.866} q_{f,inj}^{1.207} \qquad (6)$$

$$K_{1,main}\left[\frac{1}{s}\right] = 19.91\; p_f^{0.37} \rho_{SOC,main}^{0.575} n^{0.225} q_{f,inj}^{-0.69} \qquad (7)$$

$$K_{2,main}\left[\frac{s}{deg}\right] = 0.296\; p_f^{0.84} \rho_{SOC,main}^{0.59}\, n^{-0.507} K_{1,main}^{-2.12} \qquad (8)$$

$$\tau_{pil}\left[deg\right] = 257 \rho_{SOI,pil}^{-0.757}\, exp\left(\frac{1559}{T_{SOI,pil}}\right) O_2^{-1.17} \qquad (9)$$

$$\tau_{main}\left[deg\right] = 508\; p_f^{-0.648} \rho_{SOI,main}^{-0.95} O_2^{-1.265} n^{0.827} q_{f,inj}^{-0.323} \qquad (10)$$

In equations (6-10), ρ_{SOI}, $T_{SOI,}$ ρ_{SOC} and T_{SOC} indicate the in-chamber densities and temperatures evaluated at the start of injection or combustion, respectively, and are expressed in kg/m^3 and K. The injection pressure p_f is expressed in bar, the engine speed n in rpm, the total injected fuel quantity $q_{f,inj}$ (used as a load parameter) in mm^3/cyc/cyl, the total injected fuel quantity of the pilot shots $q_{pil,tot}$ in mm^3/cyc/cyl and finally the intake oxygen concentration O_2 in %. For the combustion rate parameters, the in-chamber thermodynamic conditions evaluated at SOC were selected as being more representative than those evaluated at SOI. It should be noted that it is necessary to convert the ignition delay values in 's' before their utilization in Eqs. (1-2).

Estimation of the net energy release Q_{net}

It is necessary to derive the net energy release, starting from the chemical release, in order to simulate the in-cylinder pressure during the combustion phase, taking into account the heat transfer and fuel evaporation heat effects [24]. The net heat release Q_{net} is derived from the chemical release according to the following formulation [24]:

$$Q_{net,ht} \cong Q_{ch} \frac{m_{f,inj} H_L - Q_{ht,glob}}{m_{f,inj} H_L} \qquad (11)$$

$$Q_{net} \cong Q_{net,ht} - Q_{f,evap} \qquad (12)$$

where $Q_{net,ht}$ is the result of the scaling of the chemical energy release according to the global heat exchanged by the charge with the walls, $Q_{f,evap}$ and $Q_{ht,glob}$ indicate the fuel evaporation heat from SOI to SOC (J) and the heat globally exchanged by the charge with the walls over the combustion cycle (J), and $m_{f,inj}$ is the total injected fuel mass per cycle/cylinder. The experimental values of the $Q_{f,evap}$ and $Q_{ht,glob}$ parameters were identified on the basis of the measured in-cylinder pressure traces for all the tests shown in Tab. 2 (the procedure is reported in [24], and the following correlations were identified for the two parameters as a function of the engine speed, load and intake manifold temperature:

$$Q_{f,evap}[J] = 2.22E\text{-}11\, T_{int}^{3.76} n^{0.584} q_{f,inj}^{0.270} \qquad (13)$$

$$Q_{ht,glob}[J] = 117\, n^{-0.642} q_{f,inj}^{1.50} \qquad (14)$$

Estimation of the in-cylinder pressure

The in-chamber pressure was evaluated during the combustion interval using a single-zone model [15]:

$$dp = \left(\frac{\gamma - 1}{V}\right)\left(dQ_{net} - \frac{\gamma}{\gamma - 1} pdV\right) \qquad (15)$$

where the isentropic coefficient $\gamma = c_p/c_v$ was set constant and equal to 1.37. An explicit integration method was used to solve Eq. (15), as it was verified that it leads to a good accuracy and is stable for crank angle integration steps ranging from 0.1 to 2 deg. Therefore, the adoption of implicit integration methods is not necessary.

Polytropic evolutions were assumed to calculate the in-cylinder pressure during the compression and expansion phases:

$$pV^m = const \qquad (16)$$

$$pV^{m'} = const \qquad (17)$$

The starting condition for the evaluation of the compression phase, i.e. the in-chamber pressure at IVC (Intake Valve Closure), was correlated to the pressure in the intake manifold p_{int}, using a correction factor Δp_{int}, as follows:

$$p_{IVC} = p_{int} + \Delta p_{int} \qquad (18)$$

The experimental values of the *m*, *m' and* Δp_{int} parameters were identified on the basis of the measured in-cylinder pressure traces for all the tests shown in Tab. 2 (reference can be made to [24] for the complete procedure), and the following correlations were identified for the three parameters, which are functions of the intake manifold thermodynamic conditions and of the engine load and s

peed:

$$m = 3.02\, T_{int}^{-0.173} n^{0.0167} q_{f,inj}^{0.0148} \qquad (19)$$

$$m' = 2.78\; T_{int}^{-0.0919} n^{-0.0176} q_{f,inj}^{-0.0209} \qquad (20)$$

$$\Delta p_{int}\left[bar\right] = 0.163\, p_{int}^{1.06} n^{-0.000825} q_{f,inj}^{-0.0429} \qquad (21)$$

The in-cylinder pressure values during the intake and exhaust phases were considered as constants and were set equal to the pressure in the intake and exhaust manifolds, respectively [24]. It has in fact been verified that this assumption leads to a very small error in the prediction of IMEP.

The simulation of the in-cylinder pressure traces allows several combustion parameters, such as PFP and IMEP, to be evaluated.

Estimation of FMEP

The Chen-Flynn approach [29] was adopted to estimate FMEP. This correlation takes into account the effect of the engine speed and of the peak firing pressure on the friction losses.

The experimental values of FMEP were evaluated as the difference between the experimental values of the net IMEP (obtained by means of the integration of the experimental pressure trace over the entire cycle) and the measured values of BMEP, as follows:

$$FMEP = IMEP - BMEP \quad (22)$$

As previously stated, the values of IMEP of one of the four cylinders were taken as being representative of all the cylinders, due to the low cylinder-to-cylinder dispersion.

The following correlation was identified to evaluate FMEP:

$$FMEP[bar] = -1.38E\text{-}04\ n + 6.67E\text{-}08\ n^2 + \\ +0.0126\ PFP + 1.04 \quad (23)$$

where the engine speed is expressed in rpm and PFP is expressed in bars.

The squared correlation coefficient R^2 between the predicted and experimental values of FMEP is the order of 0.89.

Estimation of the EGR rate, of the trapped mass and of the intake O_2 concentration

An empirical correlation was identified to estimate the in-cylinder trapped volume of the EGR gas (taking the EGR gas density upstream from the valve, i.e., ρ_{exh}, as the reference one), as a function of the pressure drop across the EGR valve ($\Delta p = p_{exh} - p_{int}$), of the EGR flow density at the EGR valve inlet and outlet (ρ_{int}, ρ_{exh}), of the engine speed (n), of the EGR valve opening signal (i.e., u_{EGR}), of the cooler by-pass activation flag and of the throttle valve position (i.e., u_{th}).

The proposed correlations are:

$$V_{EGR}\left[\frac{m^3}{cyc\,cyl}\right] = 6.65E\text{-}12\,\Delta p^{0.199}\rho_{int}^{-1.20}\cdot \\ \cdot\rho_{exh}^{-0.889}u_{EGR}^{0.0821}u_{th}^{-0.197}n^{2.33}\ (bypass_{EGRcooler} = OFF) \quad (24)$$

$$V_{EGR}\left[\frac{m^3}{cyc\,cyl}\right] = 5.64E\text{-}07\ \Delta p^{-0.425}\rho_{int}^{-0.960}\cdot \\ \cdot\rho_{exh}^{-0.873}u_{EGR}^{0.201}u_{th}^{2.73}n^{0.696}\ (bypass_{EGRcooler} = ON) \quad (25)$$

The squared correlation coefficient R^2 between the predicted and experimental values of the EGR trapped volume is the order of 0.93 and 0.91 for Eqs. (24-25), respectively.

In general, the trapped air and EGR mass can be evaluated on the basis of the following equation, which takes into account the volumetric efficiency λ_v:

$$m_{trap} = m_{air,trap} + m_{EGR,trap} = \lambda_v m_{trap,id} = \lambda_v \rho_{int} V_d = \lambda_v \frac{p_{int}}{RT_{int}} V_d \quad (26)$$

where ρ_{int} is the density in the intake manifold and V_d the unit displacement, p_{int} and T_{int} are the pressure and temperature in the intake manifold, respectively. The experimental values of the trapped air and EGR mass that were used to tune Eqs. (24-26) were derived from the experimental values of the relative air-to-fuel ratio λ and of the experimental EGR rate, which in turn were calculated on the basis of the measured emissions and intake manifold CO_2 concentration using the procedure explained in [30]. The experimentally-derived values of λ_v were tabulated as a function of the engine load and speed.

It can be noted that Eq. (26) is a function of the temperature in the intake manifold, which depends on the EGR rate. In general, a real-time approach should reduce as much as possible the use of iterative calculations. To this aim, an alternative empirical correlation to evaluate m_{trap} was found, which is only a function of the intake manifold pressure and engine speed:

$$m_{trap} = m_{air,trap} + m_{EGR,trap} = 430\,p_{int}^{1.10}n^{-0.0264} \quad (27)$$

The use of Eq. (27) to evaluate m_{trap} leads to a squared correlation coefficient R^2 between the predicted and experimental values of the order of 0.984, while the use of Eq. (26) leads to a value of R^2 equal to 0.990.

Once the trapped mass and the EGR mass flow rates are known, the EGR rate X_r can be evaluated as follows:

$$X_r = \frac{m_{EGR,trap}}{m_{air,trap} + m_{EGR,trap}} = \frac{\rho_{exh}V_{EGR}}{m_{trap}} \quad (28)$$

Finally, the intake oxygen concentration was evaluated as a function of the parameter X_r/λ [31-32], and the following correlation was identified:

$$O_2 = -20.353 \cdot \frac{X_r}{\lambda} + 20.786 \quad (29)$$

where λ is evaluated on the basis of the mass of injected fuel and of the mass of trapped air. The latter quantity can be obtained as the difference between the total trapped mass (Eq. (27)) and the trapped mass of EGR.

Estimation of the NOx and soot emissions

The NOx and soot emissions were evaluated starting from the semi-empirical models developed by the authors in [26-27]. These correlations were re-tuned for the engine considered in the present study, on the basis of the experimental tests reported in Tab. 2.

The following correlations were obtained from the tuning of the NOx emission model:

$$NO_x\left[ppm\right] = 24.6E{+}06\; p_f^{0.326}\; exp\left(\frac{-24500}{T_{b,MFB50}}\right) X_r^{-0.827} n^{-0.722} q_{f,inj}^{-0.0534} \qquad (X_r > 20\%)$$

(30)

$$NO_x\left[ppm\right] = 2970\; p_f^{0.307}\; exp\left(\frac{-39000}{T_{b,MFB50}}\right) O_2^{4.95} n^{-0.521} q_{f,inj}^{-0.00772} \qquad (X_r \le 20\%)$$

(31)

Equations (30-31) were derived considering all the data related to the engine map tests and variation list tests, as it was verified that this led to satisfactory results for both datasets. Moreover, at the beginning, all the main engine variables related to NOx formation were included in the correlations, and a sensitivity analysis was carried out in order to exclude the least influential ones.

The NOx concentration was used instead of the NOx mass per cycle [26] in Eqs. (30-31), as this approach led to slightly higher prediction accuracy. Moreover, the temperature of the burned gases evaluated at MFB50 (i.e., $T_{b,MFB50}$) was used instead of the maximum temperature during the combustion of the main pulse (i.e., $T_{bmax,main}$, see [26]). In fact, it was found that the utilization of the $T_{b,MFB50}$ parameter leads to the same accuracy as $T_{bmax,main}$, but it is much easier to identify in real-time applications. The temperature of the burned gases was evaluated by means of the real-time thermodynamic three-zone model presented in [33], that is summarized in the next subsection.

It is worthwhile recalling that the burned gas temperature is a very robust correlation parameter, as it is directly related to the physics of the NOx formation process (see [26]). In order to verify this, an analysis was made by re-calibrating the NOx model without using $T_{b,MFB50}$ term. As a result, it was verified that the values of the exponents of some terms increase (e.g., the exponent of the O_2 term in Eq. (31) is more than doubled), and this makes the model much less robust with respect to uncertainties in the input values.

The evaluation of the $T_{b,MFB50}$ term in general requires the evaluation of the in-cylinder pressure, which is an input of the thermodynamic model. However, for applications in which only the NOx model is requested, a correlation can be built for $T_{b,MFB50}$ (such as that presented in [26]), in order to avoid the pressure simulation.

With reference to the soot model, it was verified that a single correlation could not be used in order to obtain satisfactory results for both the engine map and variation list tests, and separate correlations were therefore identified for the two datasets. In general, the prediction of soot emissions is a quite challenging task, as the soot formation and oxidation processes depend on a high number of parameters, and this dependency is highly nonlinear (see [27]). The following correlation was identified for the variation list tests of the NEDC key-points:

$$soot\left[\frac{\mu g}{cyc\,cyl}\right] = 2.67E{-}05\; p_f^{-1.42} X_r^{1.92} (\lambda - 1)^{-0.738} Q_{ch,EOIM}^{-0.324} n^{1.86} q_{f,inj}^{3.78} \qquad (X_r > 20\%)$$

(32)

$$soot\left[\frac{\mu g}{cyc\,cyl}\right] = 3.96E{+}04\; p_f^{-1.34} X_r^{0.673} (\lambda - 1)^{-1.36} Q_{ch,EOIM}^{0.954} n^{0.562} q_{f,inj}^{-0.427} \qquad (X_r \le 20\%)$$

(33)

The correlation identified for the engine map tests is:

$$soot\left[\frac{\mu g}{cyc\,cyl}\right] = 1.20E{-}03\; p_f^{-4.67} X_r^{1.35} (\lambda - 1)^{-2.78} Q_{ch,EOIM}^{-0.913} n^{5.45} \qquad (q_{f,inj} > 30\,mm^3)$$

(34)

$$soot\left[\frac{\mu g}{cyc\,cyl}\right] = 2.22E{-}05\; p_f^{-0.356} X_r^{0.418} (\lambda - 1)^{-1.32} Q_{ch,EOIM}^{0.233} n^{2.15} \qquad (q_{f,inj} \le 30\,mm^3)$$

(35)

where $Q_{ch,EOIM}$ denotes the value of the chemical energy release evaluated at the end of the main pulse**,** a quantity that is related to the effect of the pilot pulses on the soot formation process (see [27]). The correlation parameters of the soot model were chosen on the basis of the study presented in [27]; only the most influential ones were included in order to maximize the correlation coefficient of the predicted vs. experimental trends. Moreover, the use of the (λ-1) expression instead of the λ term allowed a lower exponent to be obtained from the regression, in order to increase the robustness of the correlation.

Three-zone thermodynamic model

The real-time three-zone thermodynamic model presented in [33] has been used in order to evaluate the temperature of the burned gases, for the subsequent implementation of the NOx formation model (See Eqs. (30-31).

The combustion chamber has been divided into: a vapor-fuel zone (f), an unburned gas zone (u), made up of fresh-air, residual gas and EGR, and a burned gas zone (b) obtained from a globally stoichiometric combustion process. The combustion process can be modeled as follows. The in-cylinder content from the IVC to the SOI, is made up of unburned gas, which is considered as a homogeneous mixture of fresh air, EGR and residual gas. A vapor-fuel zone is generated after the SOI, as a consequence of the heating of the injected fuel. The parcels from the vapor fuel zone react with the parcels from the unburned gas zone at stoichiometric ratio, thus generating the burned gas zone (b) after the SOC.

The energy conservation equations are written in Eulerian nonstationary formulation for the different zones:

$$\delta Q_f + V_f dp = d\left(m_f h_f\right) - dm_{f,inj} h_{f,inj} + dm_{f\to b} h_f \qquad (36)$$

$$\delta Q_u + V_u dp = d\left(m_u h_u\right) + dm_{u\to b} h_u \qquad (37)$$

$$\delta Q_b + V_b dp = d\left(m_b h_b\right) - dm_{u\to b} h_u - dm_{f\to b} h_f \qquad (38)$$

The mass conservation equations can be written as follows:

$$dm_f = dm_{f,inj} - dm_{f\to b} \qquad (39)$$

$$dm_u = -dm_{u\to b} \qquad (40)$$

$$dm_b = dm_{u\to b} + dm_{f\to b} \qquad (41)$$

The mass transfer between adjacent zones is shown by the subscript in *dm* which consists of an arrow between the zone indexes. The specific enthalpy of the j[th] zone is denoted by h_j, $dm_{f,inj}$ is the injected fuel mass in the time interval dt, which is calculated on the basis of the injection rate profile, *p* is the in-chamber pressure, and δQ_j is the infinitesimal heat transfer between the j[th] zone and the in-chamber walls.

It is assumed that the particles in the unburned gas zone and in the vapor-fuel zone mix in stoichiometric conditions:

$$\frac{dm_{u\to b}}{dm_{f\to b}} = \alpha_{st}^{u} \qquad (42)$$

where α_{st}^{u} is the stoichiometric unburned gas-to-fuel ratio, and indicates the mass of unburned gas, that is required for a stoichiometric combustion of the unit fuel mass [33].

The burned gas zone is considered to be made up of CO_2, H_2O, O_2, N_2, O, H, OH and NO, and the dissociation effects are therefore taken into account for an accurate calculation of the burned gas temperatures. It has been verified in [33] that second-order polynomial correlations are able to accurately describe the specific enthalpy variation of the different zones, as follows:

$$h_j = a_j T_j^2 + b_j T_j + c_j \qquad (43)$$

The values of the coefficients of the enthalpy terms were derived in [33] and are not reported here for the sake of brevity.

The heat transfer terms were estimated by means of a convective and a radiative contribution, as explained in [33], the first one being modeled by the Woschni correlation.

On the basis of the procedure reported in [33], Eqs. (36-41) are then discretized considering finite time intervals $\Delta t = t^i - t^{i-1}$. It is thus possible to explicitly derive the temperature of the three zones by solving the resulting second-order polynomial equations for the three zones.

The unknowns can therefore be solved in closed form without an iterative procedure, and this allows a very low computational effort to be obtained.

Evaluation of the intake and exhaust manifold pressure and temperature

In the present study, the variables related to the intake and exhaust manifolds have been evaluated by means of correlations that were calibrated at steady-state conditions. Therefore, neither the turbocharger dynamics, nor the intake and exhaust manifold emptying and filling processes have been simulated. The pressure in the intake manifold was set equal to the set-point that was derived from the baseline engine map, which is a function of the engine load and speed:

$$p_{\text{int}} = LUT(n, q_{f,inj}) \qquad (44)$$

The intake manifold temperature (T_{int}) was evaluated by means of an enthalpy balance equation at the EGR mixing node:

$$\dot{m}_{EGR}\bar{c}_{p,EGR}T_{EGR,cout} + \dot{m}_{air}\bar{c}_{p,air}T_{air,cout} = (\dot{m}_{EGR} + \dot{m}_{air})\bar{c}_p T_{\text{int}} \qquad (45)$$

which can be rewritten as follows:

$$X_r\bar{c}_{p,EGR}T_{EGR,cout} + (1 - X_r)\bar{c}_{p,air}T_{air,cout} = \bar{c}_p T_{\text{int}} \qquad (46)$$

where $T_{EGR,cout}$ and $T_{air,cout}$ are the EGR and air temperatures at the EGR cooler and intercooler outlet, respectively. These temperatures depend on the EGR and air temperatures at the cooler inlet, as well as on the efficiencies of the coolers, which in turn depend on the engine operating conditions. The detailed evaluation of the performance of the coolers by means of specific sub-models was not carried out in this study. As a consequence, the values of the air and EGR temperatures at the outlet of the coolers were evaluated by means of look-up tables using the experimental data. It can be noted that the evaluation of T_{int} requires the EGR rate X_r, which in turn is a function of T_{int} through Eqs. (24-25, 28). A closed form evaluation of pint and EGR rate is not possible, therefore an iterative procedure has to be adopted and cannot be avoided. The squared correlation coefficient R^2 between the predicted and experimental values of T_{int} is 0.90. The exhaust manifold temperature (T_{exh}) depends on the temperature of the charge inside the cylinder at EVO (T_{EVO}), which is evaluated by means of the three-zone model, on the expansion across the exhaust valves and on the heat transfer effects between the exhaust valves and the turbine inlet. The latter effects are a function of the engine operating conditions. The following correlation has therefore been worked out:

$$T_{exh} = 9.40 T_{EVO}^{0.466} n^{0.0887} q_{f,inj}^{0.136} \qquad (47)$$

However, the application of Eq. (47) would require an iterative procedure which involves the HRR, pressure and thermodynamic models (as they are a function of T_{exh}); iterative calculations should be reduced as much as possible in a real-time approach. To this aim, an empirical evaluation of T_{exh} as a function of intake manifold pressure, SOI_{main}, engine speed and injected fuel quantity was identified, as follows:

$$T_{exh} = 15.1\, p_{\text{int}}^{-0.336} (SOI_{main} - 270)^{0.271} n^{0.0887} q_{f,inj}^{0.429} \qquad (48)$$

The use of Eq. (48) to evaluate m_{trap} leads to a squared correlation coefficient R^2 between the predicted and experimental values of the order 0.977, while the use of Eq. (47) leads to a value of R^2 equal to 0.988.

Equation (48) allows the effect of the start of injection on the exhaust gas temperatures to be taken into account.

The value of the exhaust manifold pressure (p_{exh}) is a function of the turbine expansion ratio, which depends on the boost pressure target

(i.e., p_{int}), on the turbocharger specifications and on the engine operating conditions.

For the purposes of this study p_{exh} was evaluated by means of look-up tables as a function of the intake manifold pressure, engine speed and injected fuel quantity, which were derived from the experimental data:

$$p_{exh} = LUT(p_{int}, n, q_{f,inj}) \qquad (49)$$

Summary of the real-time engine model

Figure 2 reports a synthetic flow chart of the proposed real-time engine model, in which the main input and output variables are indicated.

In general, the main input quantities of the model are the injection parameters (i.e., the injection pressure p_f, the *SOI* and the injected quantities for the different pulses) that are required to evaluate the injection rate, the engine speed n and the EGR-related variables (opening signal u_{EGR}, throttle valve opening signal u_{th}, cooler by-pass flag f_{cpb}). The variables related to the injection process were estimated by means of the ECU look-up tables, as a function of the load and speed.

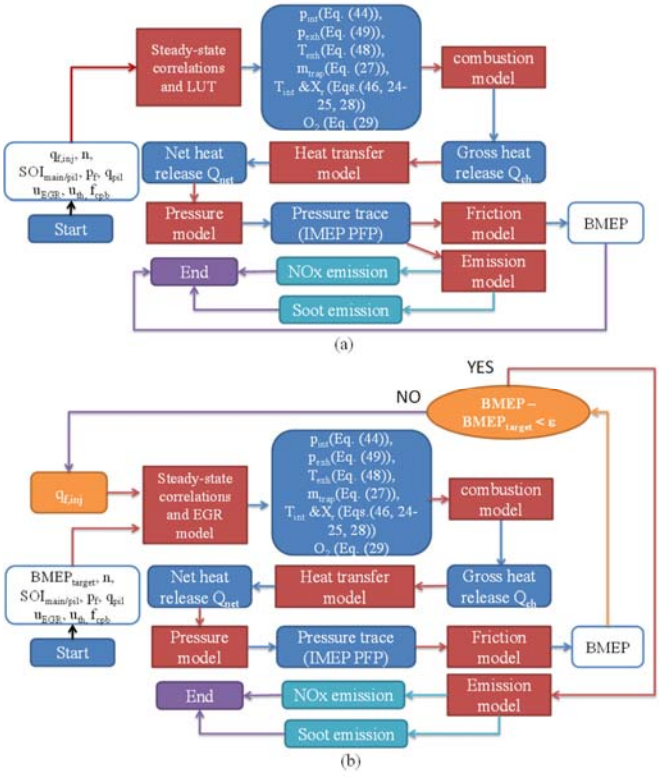

Figure 2. Flow chart of the real-time engine model, for the cases in which the total injected quantity is provided as input (a) or a BMEP target is requested as input (b).

First, the steady-state correlations and look-up tables are applied to evaluate the intake and exhaust manifold pressure (i.e., p_{int}, p_{exh}), the exhaust manifold temperature (T_{exh}) and the total trapped mass (m_{trap}); then, the evaluation of the intake manifold temperature T_{int} and of the EGR rate X_r is made by means of an iterative calculation; subsequently, the intake oxygen concentration O_2 is evaluated. The combustion model is then applied to evaluate the gross heat release (Q_{ch}), on the basis of the injection rate and of the previously evaluated quantities. The heat transfer and fuel evaporation variables are used to estimate the net heat release Q_{net}, for the subsequent calculation of the in-cylinder pressure and the related parameters (IMEP, PFP). The friction model allows FMEP to be estimated, in order to evaluate BMEP. In parallel, the emission models are used to estimate the NOx and soot emissions. If a BMEP target is required as a model input (Fig. 2b), an iterative procedure has to be applied, assuming a starting value of the injected fuel quantity $q_{f,inj}$. The values of the injected quantity are scaled iteratively according to the ratio between the target and actual values of BMEP, until convergence is achieved. It was found that an average number of 3 iterations is sufficient to achieve convergence, assuming a difference of 0.1 bar between the predicted and target values of BMEP as the convergence criterion. With this approach, the model is capable of evaluating the fuel consumption (as well as the other main output quantities) in order to achieve a BMEP target, for a given EGR rate, injection strategy and engine speed, and is therefore useful for sensitivity analyses and engine calibration tasks.

Results and discussion

Model application: steady-state conditions

The engine model was first applied to simulate the steady-state conditions reported in Tab. 2.

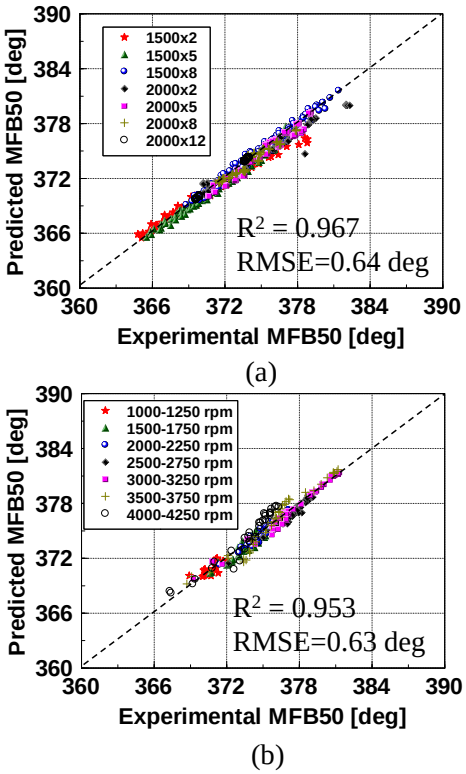

Figure 3. Predicted vs. experimental values of MFB50 obtained with the heat release model for the variation list tests (a, c) and engine map tests (b, d).

Figures 3-5 report the predicted vs. experimental values of MFB50 (Fig. 3a, b), PFP (Fig. 4a, b), BMEP (Fig. 4c, d), as well as the NOx (Fig. 5a, b) and soot emissions (Fig. 5c, d).

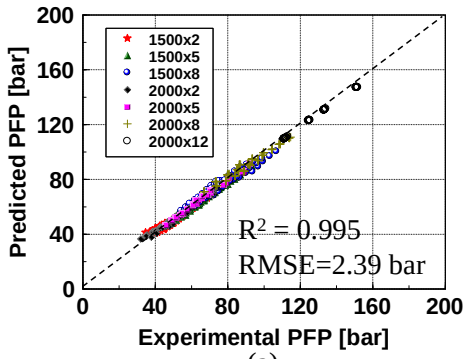

(a)

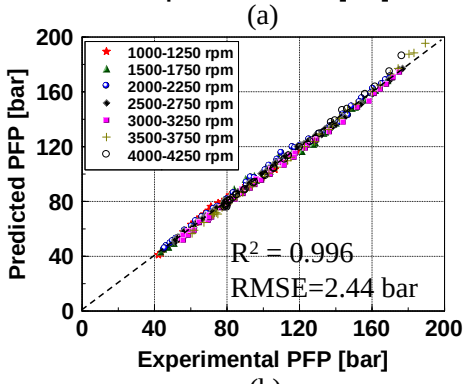

(b)

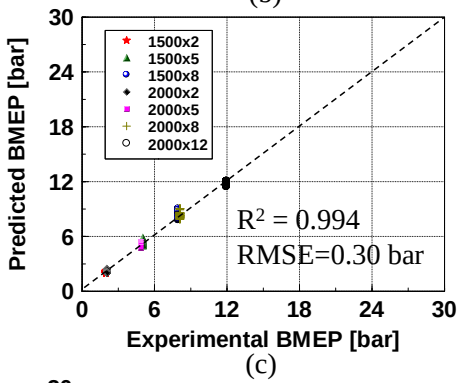

(c)

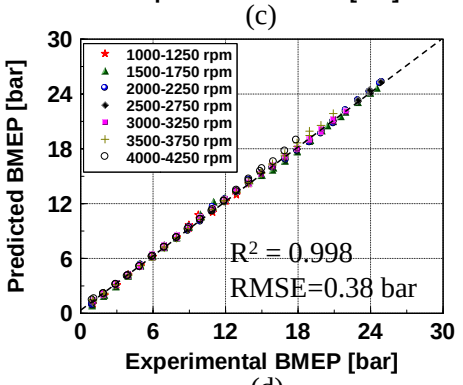

(d)

Figure 4 Predicted vs. experimental values of PFP and BMEP for the variation list tests (a, c) and engine map tests (b, d).

The results related to the variation list tests and to the engine map tests have been reported separately.

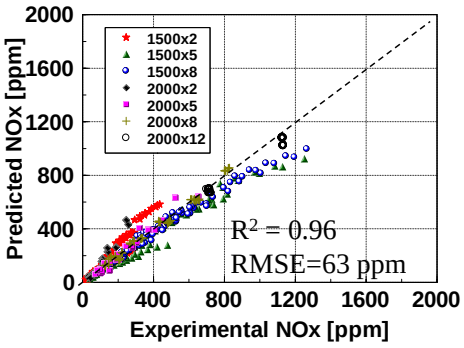

(a)

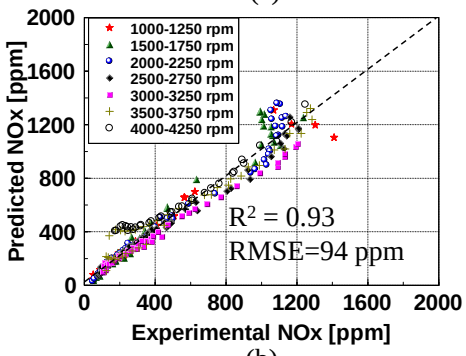

(b)

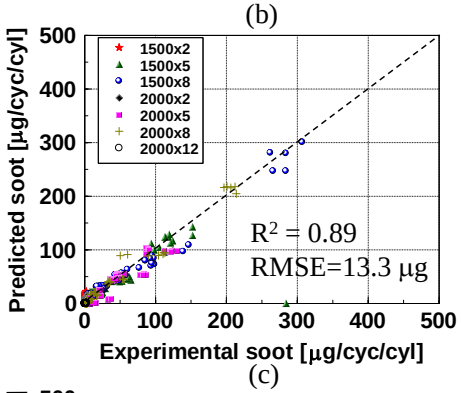

(c)

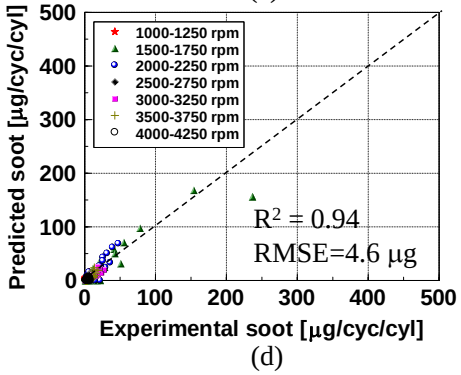

(d)

Figure 5 Predicted vs. experimental values of NOx and soot emissions for the variation list tests (a, c) and engine map tests (b, d).

The accuracy of the models was evaluated by means of the root mean square of error (RMSE) and of the squared correlation coefficient (R^2), which are reported in the graphs.

In general, it can be observed that the estimation of MFB50 is accurate, as the values of RMSE are of the order of 0.6 deg for both the variation list and engine map tests, and the correlation coefficients are of the order of 0.97 and 0.95, respectively.

A quite accurate prediction of the in-cylinder pressure is shown in Fig. 4, as the values of RMSE are of the order of 2.2-2.4 bars for the PFP, of 0.3-0.4 bars for the BMEP, and the correlation coefficients are higher than 0.99 for all the quantities.

Finally, the prediction of the NOx emissions is good for both the variation list tests and engine map tests (RMSE = 63 and 94 ppm, respectively, and the correlation coefficients are equal to 0.96 and 0.93, respectively), while the prediction of the soot emissions is quite good (RMSE = 13.3 μg and 4.6 μg, respectively, and the correlation coefficients are equal to 0.89 and 0.94, respectively).

The impact of the enhanced heat release model, recently proposed by the authors in [25] (see Eqs. (1-2)), on the prediction of the in-cylinder pressure and pollutant emissions has also been evaluated in this study, and compared with the baseline heat release model presented in [24]. The accuracy of the models was evaluated by means of the RMSE and R^2 values, which are reported in Tab. 3a. Table 3b instead reports the sum of the squared differences (SSD) of the predicted Q_{ch} and in-cylinder pressure traces with respect to the experimental ones, and is therefore an indicator of the accuracy of the prediction of the shape of the Q_{ch} and pressure profiles.

Table 3. Values of R^2 and RMSE for the main model outcomes (a) and of the SSD of the Q_{ch} and pressure profiles (b), obtained with the baseline HRR model (ref. [24]) and with the enhanced HRR model (ref. [25]).

	Variation list tests				*Engine map tests*			
	Baseline HRR model (ref. [24])		*Enhanced HRR model (ref. [25])*		*Baseline HRR model (ref. [24])*		*Enhanced HRR model (ref. [25])*	
	R^2	*RMSE*	*R^2*	*RMSE*	*R^2*	*RMSE*	*R^2*	*RMSE*
MFB50 [deg]	0.954	0.796	0.967	0.645	0.84	1.52	0.953	0.63
IMEP [bar]	0.989	0.45	0.992	0.36	0.997	0.621	0.998	0.442
PFP [bar]	0.991	3.11	0.995	2.39	0.980	10.6	0.996	2.44
BMEP [bar]	0.993	0.38	0.994	0.30	0.998	0.616	0.999	0.384
NOx [ppm]	0.966	60.3	0.964	64.5	0.879	140	0.925	109
Soot [μg/cyc/cyl]	0.892	13.4	0.893	13.3	0.948	4.75	0.946	4.57

(a)

	Variation list tests		*Engine map tests*	
	Baseline HRR model (ref. [24])	*Enhanced HRR model (ref. [25])*	*Baseline HRR model (ref. [24])*	*Enhanced HRR model (ref. [25])*
	SSD	*SSD*	*SSD*	*SSD*
Q_{ch}	411	148	1065	245
In-cylinder pressure	722	548	598	294

(b)

It was shown in [25] that the enhanced HRR model leads to a better accuracy than the baseline HRR model proposed in [24], especially in the medium-high load range. This can be confirmed by/from the results reported in Tab. 3. It can be noted that, for the engine map tests, the performance of the enhanced HRR model is better than that of the baseline HRR model, as the value of RMSE related to MFB50 is decreased from 1.5 to about 0.6 deg. This, in turns, leads to a better prediction of PFP (RMSE decreases from 10.6 to 2.4 bar), of IMEP (RMSE decreases from 0.62 to 0.44 bar), of BMEP (RMSE decreases from 0.62 to 0.38 bar), of the NOx emissions (RMSE decreases from 140 to 109 ppm) and of the soot emissions (RMSE decreases from 4.75 to 4.57 μg/cyc/cyl). As far as the engine map tests are concerned, the enhanced heat release model also leads to a better prediction not only of the Q_{ch} shape, but also of the in-cylinder pressure shape, as can be observed from the values of the SSD reported in Tab. 3b. Instead, with reference to the variation list tests, the improvement obtained with the enhanced heat release model is smaller than for the engine map tests. This is justified by the fact that the variation list tests were conducted for the key points of the NEDC that feature medium-low load conditions. However, it can be noted that the enhanced model leads to a better prediction of the heat release and pressure curves, as the values of the SSD of the Q_{ch} and in-cylinder pressure profiles are lower (see Tab. 3b).

Model application: NEDC and WLTP cycles

The performance of the real-time engine model has also been tested in transient conditions. In particular, the analysis was made over NEDC and WLTP homologation cycles, which were simulated on the dynamic test bench. The WLTP will be the reference homologation cycle for passenger cars in Europe from January 2017. The performance of the model was evaluated in terms of heat release prediction (i.e., MFB50), in-cylinder pressure prediction (i.e., PFP and IMEP) and NOx emissions. Soot emissions were not acquired during the transients, as only a smokemeter was available in the test cell. The engine was warmed up before the running of the cycles.

The results of the real-time engine model were compared with those obtained from a procedure denoted as “combustion model”. The first approach is labeled as “SS engine model” in the legend to recall that intake/exhaust variables were assessed under steady-state operating conditions. The second approach uses the experimental values of intake/exhaust variables detected during the transient. The aim of this comparison was to verify whether the assumption of using steady-state correlations to estimate the intake/exhaust variables could be accepted when moderately transient conditions, such as those of the NEDC and WLTP cycles, were simulated. Table 4 summarizes the main correlations used in the SS engine model and the measured input quantities used in the “Combustion model” approach. The simulations were performed using a CA step of 0.1 deg.

Table 4. Summary of the main correlations used in the "SS engine model" and of the measured input quantities used in the "combustion model" approach.

	SS engine model	**Combustion model**
Intake manifold p	Eq. (44)	Measured (transducer)
Intake manifold T	Eq. (46)	Measured (transducer)
Inducted charge mass (air/EGR)	Eqs. (24, 25, 27, 28)	Measured air mass (engine sensor) + measured EGR rate (based on intake CO_2)
Intake O_2 concentration	Eq. (29)	Measured (gas analyzer)
Exhaust manifold p	Eq. (49)	Measured (transducer)
Exhaust manifold T	Eq. (48)	Measured (transducer)
Injection strategy ($SOI_{main/pil}$, p_{rail}, q_{pil})	ECU maps	ECU maps
Injected quantity of the main pulse	Calculated on the basis of an iterative procedure, starting from a target of BMEP and using Eq. (23) to evaluate FMEP	ECU maps

The model outcomes, in terms of MFB50, PFP, IMEP and instantaneous/cumulated NOx emissions, are reported in Figs. 6-9 for the NEDC and in Figs. 10-13 for the WLTP.

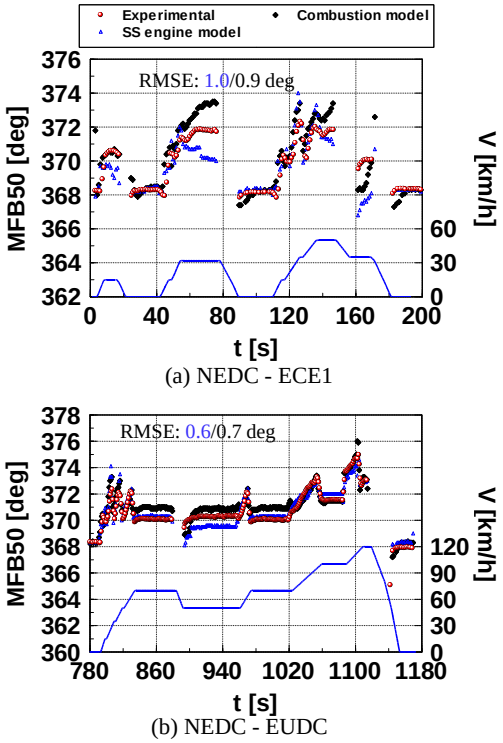

(a) NEDC - ECE1

(b) NEDC - EUDC

Figure 6 Experimental and predicted values of MFB50 obtained with the SS engine model and combustion model, over the ECE1 and EUDC phases of the NEDC cycle. The RMSE of MFB50 is also reported at the top of each graph for the SS engine model and combustion model, respectively.

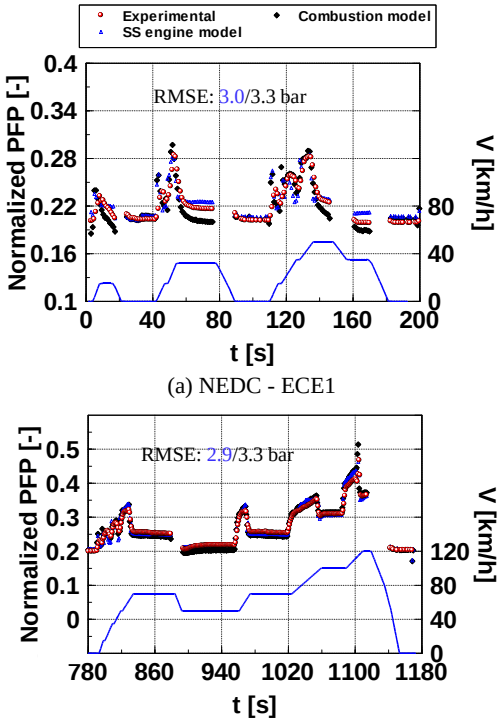

(a) NEDC - ECE1

(b) NEDC - EUDC

Figure 7 Experimental and predicted values of PFP obtained with the SS engine model and combustion model only, over the ECE1 and EUDC phases of the NEDC cycle. The RMSE of PFP is also reported at the top of each graph for the SS engine model and combustion model, respectively.

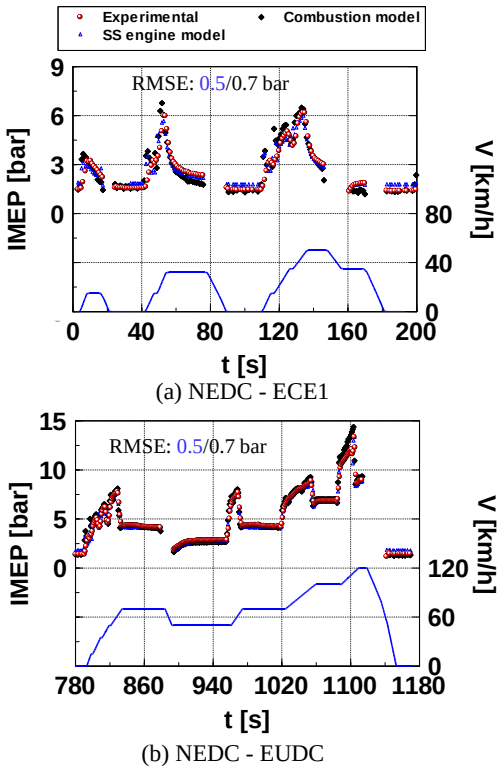

(a) NEDC - ECE1

(b) NEDC - EUDC

Figure 8 Experimental and predicted values of IMEP obtained with the SS engine model and combustion model only, over the ECE1 and EUDC phases

of the NEDC cycle. The RMSE of IMEP is also reported at the top of each graph for the SS engine model and combustion model, respectively.

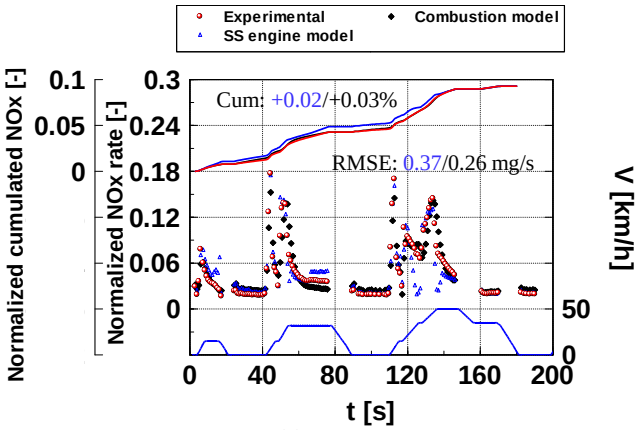

(a) NEDC - ECE1

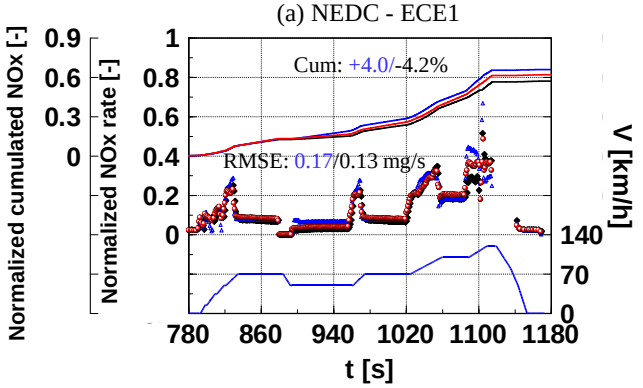

(b) NEDC - EUDC

Figure 9 Experimental and predicted values of instantaneous and cumulated NOx emissions obtained with the SS engine model and combustion model only, over the ECE1 and EUDC phases of the NEDC cycle. The RMSE of the instantaneous NOx emissions and the relative error of the cumulated NOx emissions are also reported at the top of each graph for the SS engine model and combustion model, respectively.

In all the charts, the experimental values are reported with a red circle, the results of the SS engine model with blue triangles and the results of the combustion model with black diamonds. The values of RMSE are also reported at the top of each graph for the SS engine model and combustion model, respectively. The values of PFP and NOx over the cycles were normalized for confidentiality reasons.

As far as the NEDC is concerned, the results of the ECE2-4 phases were similar to those of the ECE1, and have therefore not been reported for the sake of brevity.

Figures 6-8 report the predicted and the experimental values of MFB50, PFP and IMEP, respectively, for the ECE1 and EUDC phases of the NEDC.

It can be observed that the performance of the SS engine model and of the combustion model is very similar, in terms of heat release and in-cylinder pressure prediction, in both the urban and extra-urban phases, as the values of RMSE are very close to each other.

Figure 9 reports the predicted and experimental values of the instantaneous and normalized cumulated NOx emissions over the ECE1 (a) and EUDC (b) phases of the NEDC.

The experimental cumulated NOx emissions are indicated with red lines, the cumulated NOx emissions predicted by the SS engine model are indicated with blue lines, and the cumulated NOx emissions predicted by the combustion model are indicated with black lines. The values of RMSE of the instantaneous NOx emissions, as well as the relative error in the cumulated NOx emissions, are reported in each graph for the SS engine model and combustion model, respectively.

The SS engine model leads to the same performance accuracy as the use of the combustion model. In particular, the instantaneous and cumulated NOx mass emissions are accurate in the urban phases, while the use of the combustion model in the extra-urban phase leads to an under-estimation of the cumulated NOx emissions of about 4.2%, while the use of the real-time engine model leads to an overestimation of about +4%.

It can be concluded that the performances obtained with the two considered approaches, for both the combustion and NOx formation processes, are basically the same when NEDC is simulated.

The same comparison has been carried out for the WLTP cycle. Figures 10-13 report the predicted and the experimental values of MFB50 (Fig. 10), PFP (Fig. 11), IMEP (Fig. 12) and the instantaneous/cumulated NOx emissions (Figs. 13) for the low phase, medium phase, high phase and extra-high phase of the WLTP.

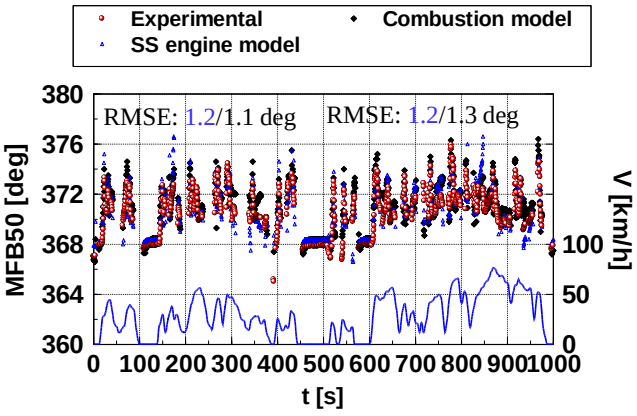

(a) WLTP: low and medium phases

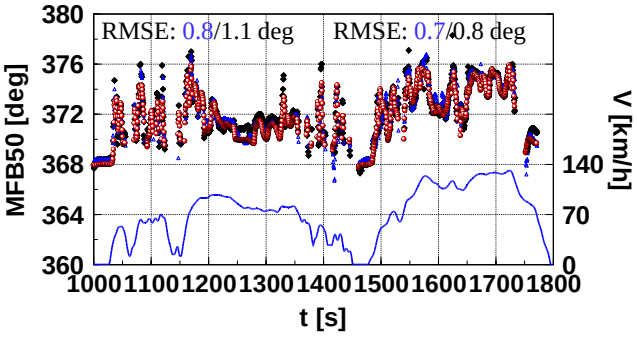

(b) WLTP: high and extra-high phases

Figure 10 Experimental and predicted values of MFB50 obtained with the SS engine model and combustion model, over the low/medium (a) and high/extra-high (b) phases of the WLTP cycle. The RMSE of MFB50 is also reported at the top of each graph for the SS engine model and combustion model, respectively.

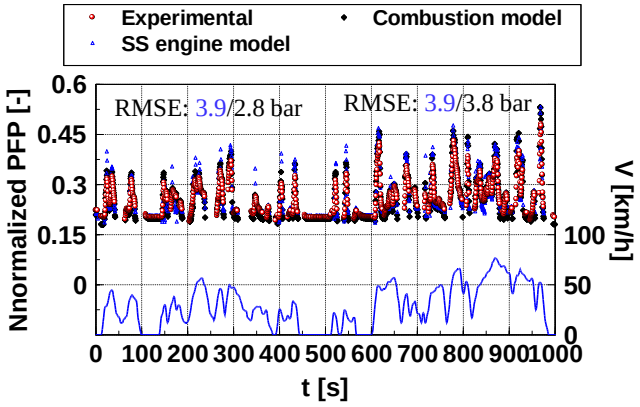

(a) WLTP: low and medium phases

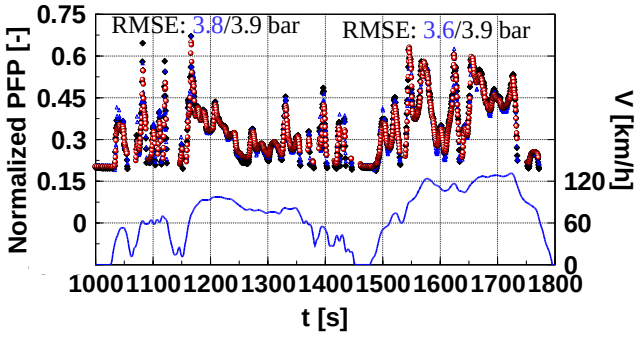

(b) WLTP: high and extra-high phases

Figure 11 Experimental and predicted values of PFP obtained with the SS engine model and combustion model, the low/medium (a) and high/extra-high (b) phases of the WLTP cycle. The RMSE of PFP is also reported at the top of each graph for the SS engine model and combustion model, respectively.

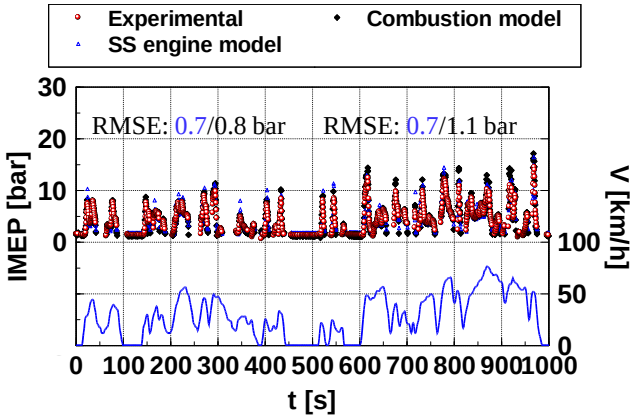

(a) WLTP: low and medium phases

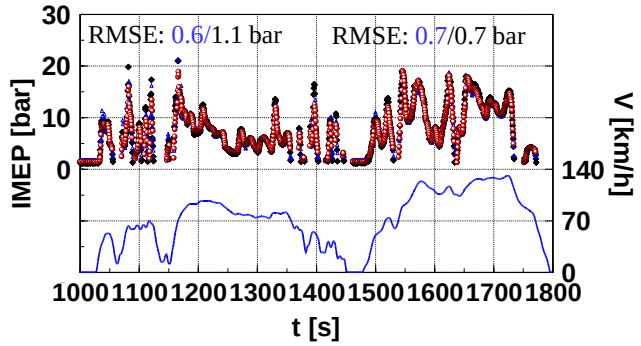

(b) WLTP: high and extra-high phases

Figure 12 Experimental and predicted values of IMEP obtained with the SS engine model and combustion model, over the low/medium (a) and high/extra-high (b) phases of the WLTP cycle. The RMSE of IMEP is also reported at the top of each graph for the SS engine model and combustion model, respectively.

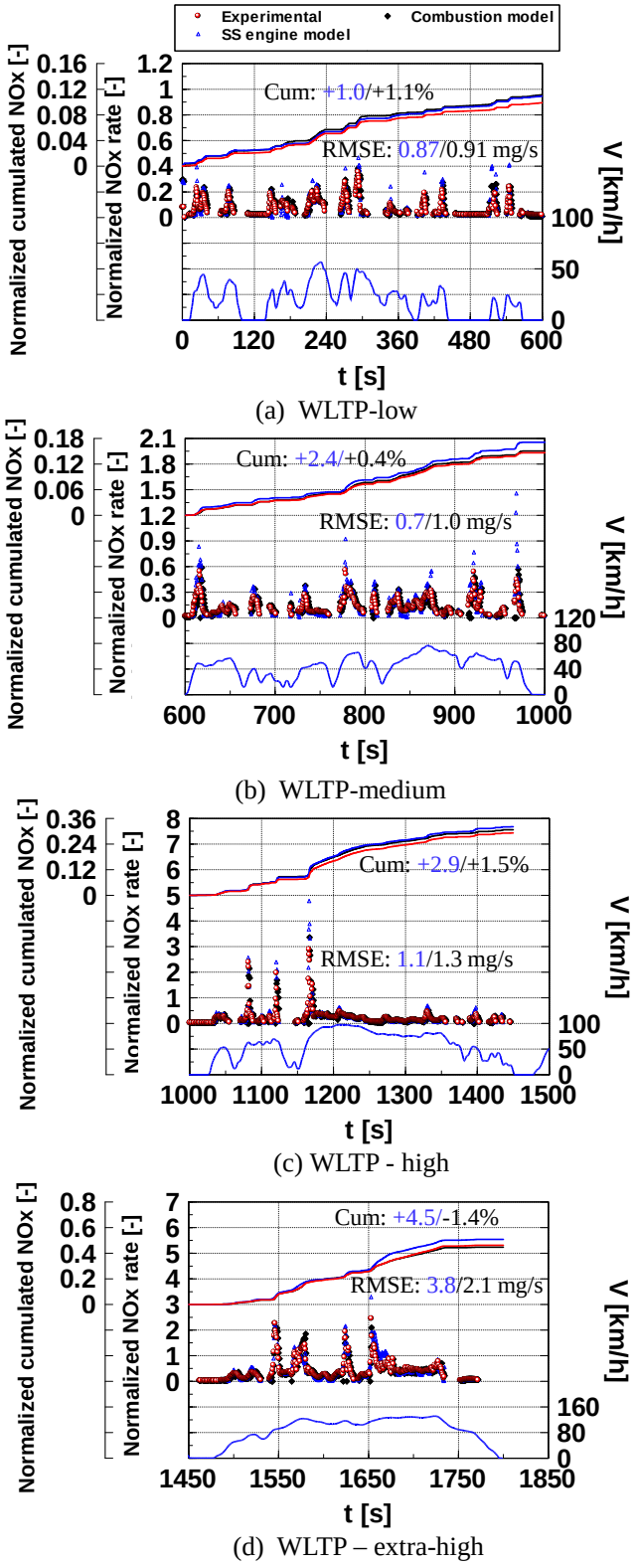

Figure 13 Experimental and predicted values of the instantaneous and cumulated NOx emissions obtained with the SS engine model and combustion model, over the low (a), medium (b), high (c) and extra-high (d) phases of the WLTP cycle. The RMSE of the instantaneous NOx emissions and the relative error of the cumulated NOx emissions are also reported at the top of each graph for the SS engine model and combustion model, respectively.

It can be observed that the performances of the SS engine model and of the combustion model for the WLTP are once again very similar, in terms of heat release, in-cylinder pressure and NOx prediction, over the entire cycle, as the RMSE values are very close to each other.

The main outcome of this analysis is that the performance of the real-time engine model leads to acceptable results when moderately-transient conditions, such as NEDC and WLTP missions, are considered.

Overall, the real-time engine model leads to a cumulated NOx emission overestimation of 2.9 % for the NEDC and of 10.8% for the WLTP. These errors are in line with previous studies reported in the literature. For example, it was shown in [34] that using a steady-state approach to calculate NOx emissions over a sequence of the ETC cycle led to an error of the order of 10%, 11% and 21% for three different heavy-duty diesel engines.

It is also interesting to note that, in that case, errors of the order of 3-4% resulted for fuel consumption, of 40-60% for CO, and of 30-50% for THC and soot emissions, using a quasi-static approach. These errors mainly derive from a deviation in the instantaneous values of the air-to-fuel ratio during the transients, with respect to the steady-state maps. A good prediction of the latter pollutant emissions in transient operation therefore requires the adoption of a transient engine model.

Computational time analysis

The computational time and the accuracy of the engine model are expected to depend to a great extent on the crank-angle step used to simulate HRR and the in-cylinder pressure; this step should be chosen on the basis of a trade-off between the calculation time and the prediction accuracy.

An analysis has therefore been carried out in order to evaluate the impact of the crank-angle step on the computational time and prediction accuracy of the main output quantities, which was quantified by the RMSE and R^2 parameters, for both the variation list and engine map tests.

The elaboration has been performed with the Labwindows CVI software, using a Pentium-D PC.

The effect of the crank-angle step on the average computational time to run a single operating condition is reported in Tab. 5

Table 5. Effect of the crank-angle step on the computational time.

Step [deg]	0.1	0.3	0.5	1.0	1.5	2
Computational time: HRR model [ms]	3.7	1.7	1.0	0.80	0.65	0.55
Computational time: pressure model [ms]	7.3	5.2	3.1	1.8	1.4	1.1
Computational time: thermodynamic and emission models [ms]	6.9	6.2	5.5	2.8	2.1	1.4

Total computational time [ms]	17.9	13.1	9.6	5.4	4.15	3.05

Tables 6-8 report the effect of the crank-angle step on the accuracy of the evaluation of MFB50 (Tab. 6), PFP and IMEP (Tab. 7), and of the NOx and soot emissions (Tab. 8).

Table 6. Effect of the crank-angle step on the accuracy of the prediction of MFB50.

MFB50 [deg]				
Step [deg]	Variation list tests		Engine map tests	
-	R^2	RMSE	R^2	RMSE
0.1	0.968	0.613	0.951	0.652
0.3	0.966	0.619	0.950	0.662
0.5	0.962	0.647	0.943	0.707
1	0.949	0.741	0.923	0.822
1.5	0.933	0.850	0.910	0.902
2	0.917	0.956	0.880	1.055

Table 7. Effect of the crank-angle step on the accuracy of the prediction of PFP and IMEP.

Step [deg]	Variation list tests				Engine map tests			
	PFP [bar]		IMEP [bar]		PFP [bar]		IMEP [bar]	
	R^2	RMSE	R^2	RMSE	R^2	RMSE	R^2	RMSE
0.1	0.995	2.39	0.992	0.36	0.996	2.44	0.998	0.442
0.3	0.995	2.32	0.992	0.421	0.996	2.4	0.998	0.573
0.5	0.995	2.42	0.993	0.511	0.995	2.56	0.998	0.727
1	0.995	2.66	0.994	0.796	0.995	2.88	0.998	1.16
1.5	0.994	3.42	0.995	1.13	0.994	3.51	0.998	1.61
2	0.991	4.12	0.995	1.47	0.991	5.11	0.998	2.13

Table 8. Effect of the crank-angle step on the accuracy of the prediction of the NOx and soot emissions.

Step [deg]	Variation list tests				Engine map tests			
	NOx [ppm]		Soot [µg/cyc/cyl]		NOx [ppm]		Soot [µg/cyc/cyl]	
	R^2	RMSE	R^2	RMSE	R^2	RMSE	R^2	RMSE
0.1	0.964	64.5	0.893	13.3	0.925	109	0.946	4.57
0.3	0.963	63.3	0.893	13.3	0.924	112	0.946	4.58
0.5	0.962	63.8	0.893	13.3	0.922	116	0.947	4.55
1	0.962	62.9	0.892	13.4	0.924	121	0.947	4.63
1.5	0.958	65.9	0.89	13.6	0.92	126	0.948	4.99
2	0.961	63.7	0.889	13.6	0.915	140	0.941	4.81

As a result of this analysis, it can be suggested not to exceed a 1.5 deg of crank-angle step in order to obtain acceptable values of RMSE. This crank-angle step value leads to a total computational time of about 4 ms.

Calibration sensitivity analysis

A sensitivity analysis has also been carried out in order to investigate the relationship between the percentage of test bench data used for the model calibration and the accuracy in the prediction of the main model output quantities. In this analysis, a certain percentage of experimental data was randomly selected to calibrate the correlations, and the model was then applied to all the available data. The percentage of calibration data was gradually decreased in order to study the corresponding influence on the model accuracy, which was quantified using the R^2 and RMSE values. The impact of the number of tests used for the calibration is reported in Tab. 9 for MFB50, in Tab. 10 for PFP/IMEP and in Tab. 11 for NOx/soot emissions.

Table 9. Values of R^2 and RMSE related to the MFB50 prediction, as a function of the percentage of available data used for the model calibration.

MFB50 [deg]				
% of available tests used for the model calibration	Variation list tests		Engine map tests	
	R^2	RMSE	R^2	RMSE
100	0.968	0.613	0.951	0.652
50	0.967	0.603	0.953	0.640
25	0.957	0.725	0.917	0.899
20	0.975	0.524	0.959	0.607
15	0.961	0.673	0.933	0.775
10	0.949	0.782	0.955	0.683
5	0.861	1.225	0.693	1.646

Table 10. Values of R^2 and RMSE related to the PFP and IMEP prediction, as a function of the percentage of available data used for the model calibration.

% of available tests used for the model calibration	Variation list tests				Engine map tests			
	PFP [bar]		IMEP [bar]		PFP [bar]		IMEP [bar]	
	R^2	RMSE	R^2	RMSE	R^2	RMSE	R^2	RMSE
100	0.995	2.39	0.992	0.36	0.996	2.44	0.998	0.442
50	0.995	2.38	0.992	0.37	0.995	2.65	0.998	0.475

25	0.995	2.34	0.992	0.338	0.996	2.75	0.998	0.407
20	0.993	2.73	0.992	0.334	0.994	3.04	0.999	0.413
15	0.996	2.73	0.992	0.357	0.99	5.23	0.998	0.496
10	0.993	2.68	0.991	0.367	0.994	3.04	0.998	0.526
5	0.994	2.44	0.994	0.339	0.988	4.38	0.999	0.435

The percentage threshold of the available data that can be used for the calibration, with a satisfactory degree of accuracy, for MFB50 resulted to be 10% in both the variation list and engine map tests (see Tab. 9). The MFB50 prediction error is unacceptable under this threshold and model accuracy is no longer guaranteed.

With reference to the in-cylinder pressure and emissions, it can be observed, in Tabs. 10-11, that the prediction of the PFP, IMEP and NOx emissions is still robust when only 5% of the available data is used, while the calibration of the soot model requires a higher number of tests, and the accuracy is almost proportional to the number of tests used for the calibration.

Table 11. Values of R^2 and RMSE related to the prediction of NOx and soot emissions, as a function of the percentage of available data used for the model calibration.

% of available tests used for the model calibration	Variation list tests				Engine map tests			
	NOx [ppm]		Soot [µg/cyc/cyl]		NOx [ppm]		Soot [µg/cyc/cyl]	
	R^2	RMSE	R^2	RMSE	R^2	RMSE	R^2	RMSE
100	0.964	64.5	0.893	13.3	0.925	109	0.946	4.57
50	0.965	60.9	0.889	13.6	0.924	115	0.942	4.68
25	0.964	62.5	0.887	13.7	0.903	120	0.9	6.3
20	0.963	70	0.831	16.8	0.912	121	0.836	7.82
15	0.958	67.5	0.853	16.1	0.932	135	0.745	10.3
10	0.96	64.4	0.733	21.3	0.915	127	0.549	13.1
5	0.947	76.4	0.634	37.2	0.888	138	0.307	17.5

Summary/Conclusions

A real-time engine model for the simulation of the HRR (heat release rate), in-cylinder pressure, BMEP (brake-mean effective pressure) and pollutant emissions, including NOx and soot, has been developed, calibrated and assessed at both steady-state and transient conditions for a Euro 6 1.6L GM diesel engine.

The chemical energy release has been simulated using an improved version of a previously developed model that is based on the accumulated fuel mass approach. The in-cylinder pressure has been evaluated on the basis of the inversion of a single-zone model. NOx and soot emissions have been simulated on the basis of semi-empirical correlations that take into account the in-cylinder thermodynamic properties, the chemical energy release and the main engine parameters.

The main thermodynamic properties in the intake and exhaust manifolds, as well as the inducted mass of air and EGR (Exhaust Gas Recirculation) have been evaluated by means of correlations and look-up tables that were calibrated at steady-state conditions, and this has allowed a very low computational time to be obtained. It can therefore be concluded that the approach is suitable for implementation in an engine ECU for real-time applications.

The model performance has been evaluated at steady-state and transient conditions. In particular, NEDC and WLTP cycles were simulated, and it has been found that the accuracy in the prediction of the heat release, in-cylinder pressure and NOx emissions is high. This suggests that the adoption of steady-state correlations to evaluate the main intake/exhaust variables is acceptable when moderately transient conditions, such as NEDC/WLTP missions, are simulated.

A sensitivity analysis has been carried out in order to evaluate the influence of the crank-angle step on the computational time and on the model accuracy. It was found that the best trade-off is achieved when a crank-angle step of the order of 1.5 deg is adopted in the simulation.

Finally, a sensitivity analysis has also been carried out in order to evaluate the influence of the number of tests used for the calibration of the models, and it has been found that only 10% of the available experimental data is sufficient to obtain high accuracy in the results. This suggests that the adopted approach is physically-consistent.

References

1. Fontanesi, F., Giacopini, M., “Multiphase CFD-CHT optimization of the cooling jacket and FEM analysis of the engine head of a V6 diesel engine”, *Applied Thermal Engineering* 52 : 293-303, 2013, doi: 10.1016/j.applthermaleng.2012.12.005.
2. Jemni, M.A., Kantchev, G., Abid, M.S., “Influence of intake manifold design on in-cylinder flow and engine performances in a bus diesel engine converted to LPG gas fuelled, using CFD analyses and experimental investigations.”, *Energy* 36:2701-2715, 2011, doi: 10.1016/j.energy.2011.02.011.
3. Lee, C.H., Reitz, R.D., “CFD simulations of diesel spray tip penetration with multiple injections and with engine compression ratios up to 100:1”, *Fuel* 111:289–297, 2013, doi: 10.1016/j.fuel.2013.04.058.
4. Perini, F., Dempsey, A., Reitz, R., Sahoo, D. et al., “A Computational Investigation of the Effects of Swirl Ratio and Injection Pressure on Mixture Preparation and Wall Heat Transfer in a Light-Duty Diesel Engine”, SAE Technical Paper 2013-01-1105, 2013, doi:10.4271/2013-01-1105.
5. Rakopoulos, C.D., Kosmadakis, G.M., Pariotis, E.G., “Investigation of piston bowl geometry and speed effects in a motored HSDI diesel engine using a CFD against a quasi-dimensional model”, *Energy Conversion and Management* 51:470–484, 2010, doi: 10.1016/j.enconman.2009.10.010.
6. Mattarellia, E., Rinaldinia, C.A., Golovitchevb, V.I., “CFD-3D Analysis of a Light Duty Dual Fuel (Diesel/Natural Gas) Combustion Engine”, *Energy Procedia* 45:929 – 937, 2014, doi: 10.1016/j.egypro.2014.01.098.
7. Mobasheri, R., Peng, Z., Mirsalim, S.M., “Analysis the effect of advanced injection strategies on engine performance and pollutant emissions in a heavy duty DI-diesel engine by CFD modeling”, *International Journal of Heat and Fluid Flow* 33:59–69, 2012, doi: 10.1016/j.ijheatfluidflow.2011.10.004.

8. Jayashankara, B., Ganesan, V., “Effect of fuel injection timing and intake pressure on the performance of a DI diesel engine – A parametric study using CFD”, *Energy Conversion and Management* 51:1835–1848, 2010, doi: 10.1016/j.enconman.2009.11.006.
9. Cipolla, G., Vassallo, A., Catania, A., Spessa, E. et al., "Combined application of CFD modeling and pressure-based combustion diagnostics for the development of a low compression ratio high-performance diesel engine" SAE Technical Paper 2007-24-0034, 2007, doi:10.4271/2007-24-0034.
10. Lešnik, L., Iljaz, J., Hribernik, A., Kegl, B., “Numerical and experimental study of combustion, performance and emission characteristics of a heavy-duty DI diesel engine running on diesel, biodiesel and their blends”, *Energy Conversion and Management* 81:534–546, 2014, doi: 10.1016/j.enconman.2014.02.039.
11. Kéromnès, A., Delaporte, B., Schmitz, G., Le Moyne, L., “Development and validation of a 5 stroke engine for range extenders application”, *Energy Conversion and Management* 82:259–267, 2014, doi: 10.1016/j.enconman.2014.03.025.
12. Arcidiacono, M., Baratta, M., Finesso, R., Kheshtinejad, H. et al., "Use of an Innovative Predictive Heat Release Model Combined to a 1D Fluid-Dynamic Model for the Simulation of a Heavy Duty Diesel Engine," *SAE Int. J. Engines* 6(3):1566-1579, 2013, doi:10.4271/2013-24-0012.
13. Montenegro, G., Onorati, A., Piscaglia, F., D'Errico, G., "Integrated 1D-MultiD Fluid Dynamic Models for the Simulation of I.C.E. Intake and Exhaust Systems", SAE Technical Paper 2007-01-0495, 2007, doi: 10.4271/2007-01-0495.
14. Arsie, I., Cricchio, A., Pianese, C., De Cesare, M., “Real-Time Estimation of Intake O2 Concentration in Turbocharged Common-Rail Diesel Engines”, SAE Technical Paper 2013-01-0343, 2013, doi: 10.4271/2013-01-0343.
15. Heywood, J.B., “Internal Combustion Engine Fundamentals”, McGraw-Hill Intern. Editions, 1988.
16. Ponti, F., Corti, E., Serra, G., De Cesare, M., “Common Rail Multi-Jet Diesel Engine Combustion Model Development for Control Purposes”, SAE Technical Paper 2007-01-0383, 2007, doi:10.4271/2007-01-0383.
17. Ponti, F., Ravaglioli, V., Moro, D., Serra, G., “MFB50 On-Board Evaluation Based on a Zero-Dimensional ROHR Model”, SAE Technical Paper 2011-01-1420, 2011, doi:10.4271/2011-01-1420.
18. Arrègle, J., García, J.M., López, J.J., Fenollosa, C., “Development of a zero-dimensional Diesel combustion model. Part 1: Analysis of the quasi-steady diffusion combustion phase”, *Applied Thermal Engineering.* 23(11):1301-1317, 2003, doi:10.1016/S1359-4311(03)00079-6.
19. Arrègle, J., García, J.M., López, J.J., Fenollosa, C., “Development of a zero-dimensional Diesel combustion model. Part 2: Analysis of the transient initial and final diffusion combustion phases”, *Applied Thermal Engineering.* 23(11):1319-1331, 2003, doi:10.1016/S1359-4311(03)00080-2.
20. Chmela, F.G., and Orthaber, G.C., “Rate of Heat Release Prediction for Direct Injection Diesel Engines Based on Purely Mixing Controlled Combustion”, SAE Technical Paper 1999-01-0186, 1999, doi:10.4271/1999-01-0186.
21. Egnell, R., “A Simple Approach to Studying the Relation between Fuel Rate, Heat Release Rate and NO Formation in Diesel Engines”, SAE Technical Paper 1999-01-3548, 1999, doi:10.4271/1999-01-3548.
22. Ryan, T. W., Callahan, T.J., “Homogeneous Charge Compression Ignition of Diesel Fuels”. SAE Technical Paper 961160, 1996, doi:10.4271/961160.
23. Ericson, C., Westerberg, B., Andersson, M., and Egnell, R., “Modelling Diesel Engine Combustion and NOx Formation for Model Based Control and Simulation of Engine and Exhaust Aftertreatment Systems”, SAE Technical Paper 2006-01-0687, 2006, doi:10.4271/2006-01-0687.
24. Catania, A.E., Finesso, R., Spessa, E., “Predictive Zero-Dimensional Combustion Model for DI Diesel Engine Feed-Forward Control”, *Energy Conversion and Management.* 52(10):3159–3175, 2011, doi:10.1016/j.enconman.2011.05.003.
25. Alfieri V, Conte G, Finesso R, Spessa E, Yang Y., “HRR and MFB50 Estimation in a Euro 6 Diesel Engine by means of Control-Oriented Predictive Models”, SAE Technical paper 2015-01-0879, doi: doi:10.4271/2015-01-0879.
26. D’Ambrosio, S., Finesso, R., Fu, L., Mittica, A., Spessa, E., “A Control-Oriented Real-Time Semi-Empirical Model for the Prediction of NOx Emissions in Diesel Engines”, *Applied Energy* 130:265-279; 2014,.doi: 10.1016/j.apenergy.2014.05.046.
27. Finesso, R., Misul, D,A., Spessa, E., “Development and Validation of a Semiempirical Model for the Estimation of Particulate Matter in Diesel Engines”, Energy Conversion and Management 84:374-389, 2014. doi: 10.1016/j.enconman.2014.04.053.
28. Finesso, R., Spessa, E., “Ignition delay prediction of multiple injections in diesel engines”, Fuel 119(1):170-190, 2014, doi: 10.1016/j.fuel.2013.11.040.
29. Chen, S.K., Flynn, P.F., “Development of Single Cylinder Compression Ignition Research Engine”, SAE Technical Paper 650733, 1966. doi:10.4271/650733.
30. d'Ambrosio, S., Finesso, R., Spessa, E., “Calculation of Mass Emissions, Oxygen Mass Fraction and Thermal Capacity of the Inducted Charge in SI and Diesel Engines from Exhaust and Intake Gas Analysis”, *Fuel* 90:152-166, 2011. doi: 10.1016/j.fuel.2010.08.025, 2011.
31. Nakayama, S., Fukuma, T., Matsunaga, A., Miyake, T, et al, “A New Dynamic Combustion Control Method Based on Charge Oxygen Concentration for Diesel Engines”, SAE Technical Paper 2003-01-3181, 2003, doi:10.4271/2003-01-3181.
32. Nakayama, S., Ibuki, T., Hosaki, H., Tominaga, H., “An Application of Model Based Combustion Control to Transient Cycle-by-Cycle Diesel Combustion”, SAE Technical Paper 2008-01-1311, 2008, doi:10.4271/2008-01-1311.
33. Finesso, R., Spessa E., “Real-Time Predictive Modeling of Combustion and NOx Formation in Diesel Engines Under Transient Conditions”, SAE Technical Paper 2012-01-0899, 2012, doi:10.4271/2012-01-0899.
34. Ericson, C., Westerberg, B., and Egnell, R., "Transient Emission Predictions With Quasi Stationary Models," SAE Technical Paper 2005-01-3852, 2005, doi:10.4271/2005-01-3852.

Contact Information

Ezio Spessa (Associate Professor)

IC Engines Advanced Laboratory

Dipartimento Energia, Politecnico di Torino

c.so Duca degli Abruzzi, 24 - 10129 Torino (Italy)

phone: +39-011-090.4482

ezio.spessa@polito.it.

Acknowledgments

Dr. Giuseppe Conte, Dr. Vincenzo Alfieri and GMPT-E are kindly acknowledged for the technical support in the activities.

Definitions/Abbreviations

BMEP	Brake Mean Effective Pressure
CA	crank angle
CFD	Computer Fluid-Dynamics
c_p	specific heat at constant pressure
c_v	specific heat at constant volume
ECE	urban phase of the NEDC cycle
ECU	Engine Control Unit
EGR	Exhaust Gas Recirculation
EOI	end of injection
EUDC	extra-urban driving cycle
f_{cbp}	cooler by-pass flag
FEM	Finite Element Method
FMEP	Friction Mean Effective Pressure
GMPT-E	General Motors PowerTrain-Europe
h	specific enthalpy
H_L	lower heating value of the fuel
HRR	Heat Release Rate
IMEP	Indicated Mean Effective Pressure
IVC	Intake Valve Closing
K	combustion rate coefficient
LUT	look-up table
m	mass; compression phase polytropic coefficient
m'	expansion phase polytropic coefficient
$\dot{m}_{f,inj}$	fuel injection rate
MFB50	crank angle at which 50% of the fuel mass fraction has burned
n	engine rotational speed
NEDC	New European Driving Cycle
O_2	intake charge oxygen concentration
p	pressure
p_f	injection pressure
p_{int}	intake manifold pressure
pil	pilot injection
q	injected fuel volume quantity
Q_{ch}	chemical heat release
$Q_{f,evap}$	energy associated to fuel evaporation
Q_{fuel}	chemical energy associated with the injected fuel
$Q_{ht,glob}$	global heat transfer between the charge and the walls
Q_{net}	net heat release
$q_{f,inj}$	total injected fuel volume quantity
q_{pil}	injected fuel volume quantity of the pilot injection
$q_{pil,tot}$	total injected fuel volume quantity of the pilot injections
R	gas constant
R^2	squared correlation coefficient
RMSE	root mean square error
SOC	start of combustion
SOI	electric start of Injection
SSD	sum of squared differences
t	time

T	temperature
T_{int}	intake manifold temperature
u_{EGR}	EGR valve opening signal
u_{th}	throttle valve opening signal
V	volume
V_d	unit displacement
VGT	Variable Geometry Turbocharger
X_r	EGR rate
WLTP	Worldwide harmonized Light-duty Testing Procedure

Greek symbols

α_{st}^{u}	stoichiometric unburned-to-fuel ratio
$\gamma = c_p/c_v$	specific heat ratio
λ	relative air-to-fuel ratio
λ_v	volumetric efficiency
ρ	density
ρ_{SOI}	in-chamber ambient density evaluated at the SOI instant
ρ_{SOC}	in-chamber ambient density evaluated at the SOC instant
τ_{main}	ignition delay of the main pulse
τ_{pil}	ignition delay of the pilot pulse